2. DIFFRACTION GEOMETRY AND ITS PRACTICAL REALIZATION

distance between the X-ray tube focus and the crystal, and η the crystal mosaic spread (Fig. 2.2.7.1).

In the moving-crystal method, Δ is the minimum angle through which the crystal must be rotated, for a given reflection, so that every mosaic block can diffract radiation covering a fixed wavelength band $\delta\lambda$ from every point on the focal spot.

This angle Δ can be controlled to some extent, for the protein case, by collimation. For example, with a collimator entrance slit placed as close to the X-ray tube source and a collimator exit slit placed as close to the sample as possible, the value of $(a+f)/s$ can approximately be replaced by $(a'+f')/s'$, where f' is the entrance-slit size, a' is the exit-slit size, and s' the distance between them. Clearly, for $a' < a$, the whole crystal is no longer bathed by the X-ray beam. In fact, by simply inserting horizontal and vertical adjustable screws at the front and back of the collimator, adjustment to the horizontal and vertical divergence angles can be made. The spot size at the detector can be calculated approximately by multiplying the particular reflection rocking angle Δ by the distance from the sample to the spot on the detector. In the case of a single-counter diffractometer, tails on a diffraction spot can be eliminated by use of a detector collimator.
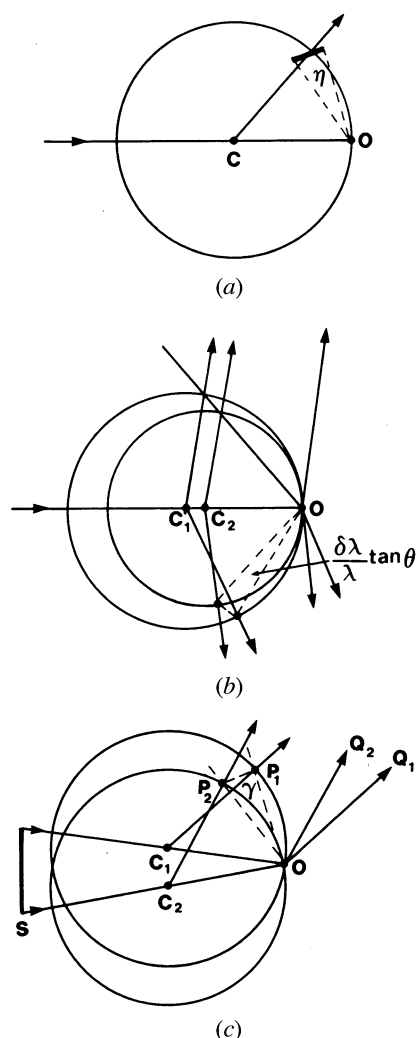

(*a*)

(*b*)

(*c*)

Fig. 2.2.7.1. Reflection rocking width for a conventional X-ray source. From Arndt & Wonacott (1977, p. 7). (*a*) Effect of sample mosaic spread. The relp is replaced by a spherical cap with a centre at the origin of reciprocal space where it subtends an angle η. (*b*) Effect of $(\delta\lambda/\lambda)_{\mathrm{conv}}$, the conventional source type spectral spread. (*c*) Effect of a beam divergence angle, γ. The overall reflection rocking width is a combination of these effects.

Spot-to-spot spatial resolution can be enhanced by use of focusing mirrors, which is especially important for large-protein and virus crystallography, where long cell axes occur. The effect is achieved by focusing the beam on the detector, thereby changing a divergence from the source into a convergence to the detector.

In the absence of absorption, at grazing angles, X-rays up to a certain critical energy are reflected. The critical angle θ_c is given by

$$\theta_c = \left[\frac{e^2}{mc^2}\frac{N}{\pi}\right]^{1/2}\lambda, \qquad (2.2.7.3)$$

where N is the number of free electrons per unit volume of the reflecting material. The higher the atomic number of a given material then the larger is θ_c for a given critical wavelength. The product of mirror aperture with reflectivity gives a figure of merit for the mirror as an efficient optical element.

The use of a pair of perpendicular curved mirrors set in the horizontal and vertical planes can focus the X-ray tube source to a small spot at the detector. The angle of the mirror to the incident beam is set to reject the $K\beta$ line (and shorter-wavelength *Bremsstrahlung*). Hence, spectral purity at the sample and diffraction spot size at the detector are improved simultaneously. There is some loss of intensity (and lengthening of exposure time) but the overall signal-to-noise ratio is improved. The primary reason for doing this, however, is to enhance spot-to-spot spatial resolution even with the penalty of the exposure time being lengthened. The rocking width of the sample is not affected in the case of 1:1 focusing (object distance $=$ image distance). Typical values are tube focal-spot size, $f = 0.1\,\mathrm{mm}$, tube-to-mirror and mirror-to-sample distances $\sim 200\,\mathrm{mm}$, convergence angle $2\,\mathrm{mrad}$, and focal-spot size at the detector $\sim 0.3\,\mathrm{mm}$.

To summarize, the configurations are

(*a*) beam collimator only;

(*b*) filter + beam collimator;

(*c*) filter + beam collimator + detector collimator (single-counter case);

(*d*) graphite monochromator + beam collimator;

(*e*) pair of focusing mirrors + exit-slit assembly;

(*f*) focusing germanium monochromator + perpendicular focusing mirror + exit-slit assembly.

(*a*) is for Laue mode; (*b*)–(*f*) are for monochromatic mode; (*f*) is a fairly recent development for conventional-source work.

2.2.7.3. *Synchrotron X-ray sources*

In the utilization of synchrotron X-radiation (SR), both Laue and monochromatic modes are important for data collection. The unique geometric and spectral properties of SR renders the treatment of diffraction geometry different from that for a conventional X-ray source. The properties of SR are dealt with in Subsection 4.2.1.5 and elsewhere; see Subject Index. Reviews of instrumentation, methods, and applications of synchrotron radiation in protein crystallography are given by Helliwell (1984, 1992).

(*a*) *Laue geometry: sources, optics, sample reflection bandwidth, and spot size*

Laue geometry involves the use of the fully polychromatic SR spectrum as transmitted through the beryllium window that is used to separate the apparatus from the machine vacuum. There is useful intensity down to a wavelength minimum of $\sim \lambda_c/5$, where λ_c is the critical wavelength of the magnet source. The maximum wavelength is typically $\geq 3\,\text{Å}$; however, if the crystal

38

is mounted in a capillary then the glass absorbs the wavelengths beyond ~ 2.6 Å.

The bandwidth can be limited somewhat under special circumstances. A reflecting mirror at grazing incidence can be used for two reasons. First, the minimum wavelength in the beam can be sharply defined to aid the accurate definition of the Laue-spot multiplicity. Second, the mirror can be used to focus the beam at the sample. The maximum-wavelength limit can be truncated by use of aluminium absorbers of varying thickness or by use of a transmission mirror (Lairson & Bilderback, 1992; Cassetta *et al.*, 1993).

The measured intensity of individual Laue diffraction spots depends on the wavelength at which they are stimulated. The problem of wavelength normalization is treated by a variety of methods. These include:

(*a*) use of a monochromatic reference data set;

(*b*) use of symmetry equivalents in the Laue data set recorded at different wavelengths;

(*c*) calibration with a standard sample such as a silicon crystal. Each of these methods produces a 'λ-curve' describing the relative strength of spots measured at various wavelengths. The methods rely on the incident spectrum being smooth and stable with time. There are discontinuities in the 'λ-curve' at the bromine and silver *K*-absorption edges owing to the silver bromide in the photographic emulsion case. The λ-curve is therefore usually split up into wavelength regions, *i.e.* $\lambda_{\min}$ to 0.49 Å, 0.49 to 0.92 Å, and 0.92 Å to $\lambda_{\max}$. Other detector types have different discontinuities, depending on the material making up the X-ray absorbing medium. [The quantification of conventional-source Laue-diffraction data (Rabinovich & Lourie, 1987; Brooks & Moffat, 1991) requires the elimination of spots recorded near the emission-line wavelengths.]

The production and use of narrow-bandpass beams may be of interest, *e.g.* $\delta\lambda/\lambda \leq 0.2$. Such bandwidths can be produced by a combination of a reflection mirror used in tandem with a transmission mirror. Alternatively, an X-ray undulator of 10–100 periods ideally should yield a bandwidth behind a pinhole of $\delta\lambda/\lambda \simeq 0.1$–0.01. In these cases, wavelength normalization is more difficult because the actual spectrum over which a reflection is integrated is rapidly varying in intensity. The spot bandwidth is determined by the mosaic spread and horizontal beam divergence (since $\gamma_H > \gamma_V$) as

$$\left[\frac{\delta\lambda}{\lambda}\right] = (\eta + \gamma_H)\cot\theta, \qquad (2.2.7.4)$$

where η = sample mosaic spread, assumed to be isotropic, γ_H = horizontal cross-fire angle, which in the absence of focusing is $(x_H + \sigma_H)/P$, where x_H is the horizontal sample size and σ_H the horizontal source size, and P is the sample to the tangent-point distance; and similarly for γ_V in the vertical direction. Generally, at SR sources, σ_H is greater than σ_V. When a focusing-mirror element is used, γ_H and/or γ_V are convergence angles determined by the focusing distances and the mirror aperture.

The size and shape of the diffraction spots vary across the film. The radial spot length is given by convolution of Gaussians as

$$(L_R^2 + L_c^2 \sec^2 2\theta)^{1/2} \qquad (2.2.7.5)$$

and tangentially by

$$(L_T^2 + L_c^2)^{1/2}, \qquad (2.2.7.6)$$

where L_c is the size of the X-ray beam (assumed circular) at the sample, and

$$L_R = D\sin(2\eta + \gamma_R)\sec^2 2\theta \qquad (2.2.7.7)$$

$$L_T = D(2\eta + \gamma_T)\sin\theta\sec 2\theta, \qquad (2.2.7.8)$$

and

$$\gamma_R = \gamma_V \cos\psi + \gamma_H \sin\psi \qquad (2.2.7.9)$$

$$\gamma_T = \gamma_V \sin\psi + \gamma_H \cos\psi, \qquad (2.2.7.10)$$

where ψ is the angle between the vertical direction and the radius vector to the spot (see Andrews, Hails, Harding & Cruickshank, 1987). For a crystal that is not too mosaic, the spot size is dominated by L_c. For a mosaic or radiation-damaged crystal, the main effect is a radial streaking arising from η, the sample mosaic spread.

(*b*) Monochromatic SR beams: optical configurations and sample rocking width

A wide variety of perfect-crystal monochromator configurations are possible and have been reviewed by various authors (Hart, 1971; Bonse, Materlik & Schröder, 1976; Hastings, 1977; Kohra, Ando, Matsushita & Hashizume, 1978). Since the reflectivity of perfect silicon and germanium is effectively 100%, multiple-reflection monochromators are feasible and permit the tailoring of the shape of the monochromator resolution function, harmonic rejection, and manipulation of the polarization state of the beam. Two basic designs are in common use. These are (*a*) the bent single-crystal monochromator of triangular shape (Lemonnier, Fourme, Rousseaux & Kahn, 1978) and (*b*) the double-crystal monochromator.
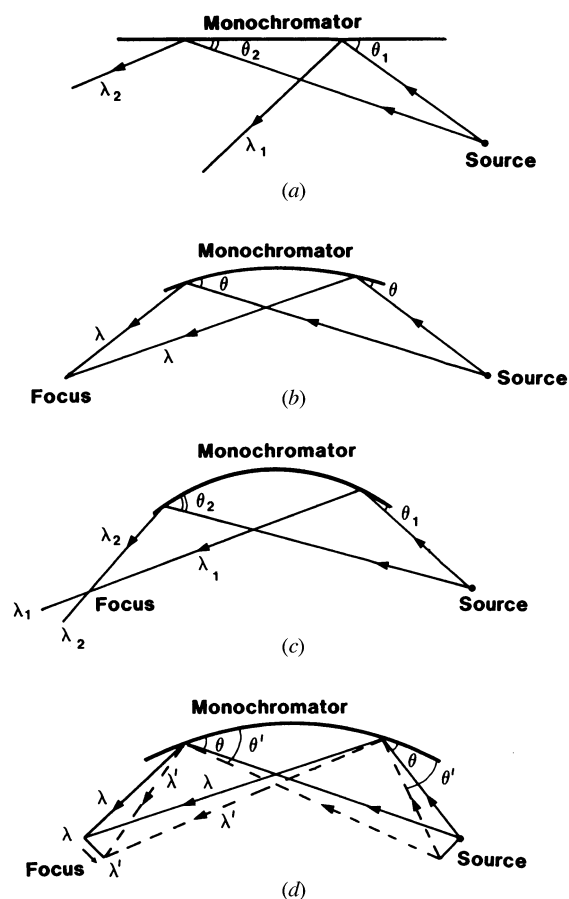

Fig. 2.2.7.2. Single-crystal monochromator illuminated by synchrotron radiation: (*a*) flat crystal, (*b*) Guinier setting, (*c*) overbent crystal, (*d*) effect of source size (shown at the Guinier setting for clarity). From Helliwell (1984).

39

In the case of the single-crystal monochromator, the actual curvature employed is very important in the diffraction geometry. For a point source and a flat monochromator crystal, there is a gradual change in the photon wavelength selected from the white beam as the length of the monochromator is traversed [Fig. 2.2.7.2(a)]. For a point source and a curved monochromator crystal, one specific curvature can compensate for this variation in incidence angle [Fig. 2.2.7.2(b)]. The reflected spectral bandwidth is then at a minimum; this setting is known as the 'Guinier position'. If the curvature of the monochromator crystal is increased further, a range of photon wavelengths, $(\delta\lambda/\lambda)_{corr}$, is selected along its length so that the rays converging towards the focus have a correlation of photon wavelength and direction [Fig. 2.2.7.2(c)]. The effect of a finite source is to cause a change in incidence angle at the monochromator crystal, so that at the focus there is a photon-wavelength gradient across the width of the focus (for all curvatures) [Fig. 2.2.7.2(d)]. The use of a slit in the focal plane is akin to placing a slit at the tangent point to limit the source size.

The double-crystal monochromator with two parallel or nearly parallel perfect crystals of germanium or silicon is a common configuration. The advantage of this is that the outgoing monochromatic beam is parallel to the incoming beam, although it is slightly displaced vertically by an amount $2d\cos\theta$, where d is the perpendicular distance between the crystals and θ the monochromator Bragg angle. The monochromator can be rapidly tuned, since the diffractometer or camera need not be re-aligned significantly in a scan across an absorption edge. Between absorption edges, some vertical adjustment of the diffractometer is required. Since the rocking width of the fundamental is broader than the harmonic reflections, the strict parallelism of the pair of crystal planes can be relaxed, *i.e.* detuned so that the harmonic can be rejected with little loss of the fundamental intensity. The spectral spread in the reflected monochromatic beam is determined by the source divergence accepted by the monochromator, the angular size of the source, and the monochromator rocking width (see Fig. 2.2.7.3).

The double-crystal monochromator is often used with a toroid focusing mirror; the functions of monochromatization are then separated from the focusing (Hastings, Kincaid & Eisenberger, 1978).

The rocking width of a reflection depends on the horizontal and vertical beam divergences/convergences (after due account for collimation is taken) γ_H and γ_V, the spectral spreads $(\delta\lambda/\lambda)_{conv}$ and $(\delta\lambda/\lambda)_{corr}$, and the mosaic spread η. We assume that $\eta \gg \omega$, where ω is the angular broadening of a relp due to a finite sample. In the case of synchrotron radiation, γ_H and γ_V are usually widely asymmetric. On a conventional source, usually $\gamma_H \simeq \gamma_V$.

Two types of spectral spread occur with synchrotron and neutron sources. The term $(\delta\lambda/\lambda)_{conv}$ is the spread that is passed down each incident ray in a divergent or convergent incident beam; the subscript refers to conventional source type. This is because it is similar to the $K\alpha_1$, $K\alpha_2$ line widths and separation. At the synchrotron, this component also exists and arises from the monochromator rocking width and finite-source-size effects. The term $(\delta\lambda/\lambda)_{corr}$ is special to the synchrotron or neutron case. The subscript 'corr' refers to the fact that the ray direction can be correlated with the photon or neutron wavelength. Usually, an instrument is set to have $(\delta\lambda/\lambda)_{corr} = 0$. In the most general case, for a $(\delta\lambda/\lambda)_{corr}$ arising from the horizontal ray direction correlation with photon energy, and the case of a horizontal rotation axis, then the rocking width φ_R of an individual reflection is given by

$$\varphi_R = \left\{ L^2\left[\left(\frac{\delta\lambda}{\lambda}\right)_{corr} d^{*2} + \zeta\gamma_H \right]^2 + \gamma_V^2 \right\}^{1/2} + 2\varepsilon_s L, \quad (2.2.7.11)$$

where

$$\varepsilon_s = \frac{d^*\cos\theta}{2}\left[\eta + \left(\frac{\delta\lambda}{\lambda}\right)_{conv}\tan\theta \right] \quad (2.2.7.12)$$

and L is the Lorentz factor $1/(\sin^2 2\theta - \zeta^2)^{1/2}$.

The Guinier setting of the instrument gives $(\delta\lambda/\lambda)_{corr} = 0$. The equation for φ_R then reduces to

$$\varphi_R = L[(\zeta^2\gamma_H^2 + \gamma_V^2/L^2)^{1/2} + 2\varepsilon_s] \quad (2.2.7.13)$$

(from Greenhough & Helliwell, 1982). For example, for $\zeta = 0$, $\gamma_V = 0.2$ mrad (0.01°), $\theta = 15°$, $(\delta\lambda/\lambda)_{conv} = 1 \times 10^{-3}$ and $\eta = 0.8$ mrad (0.05°), then $\varphi_R = 0.08°$. But φ_R increases as ζ increases [see Greenhough & Helliwell (1982, Table 5)].

In the rotation/oscillation method as applied to protein and virus crystals, a small angular range is used per exposure
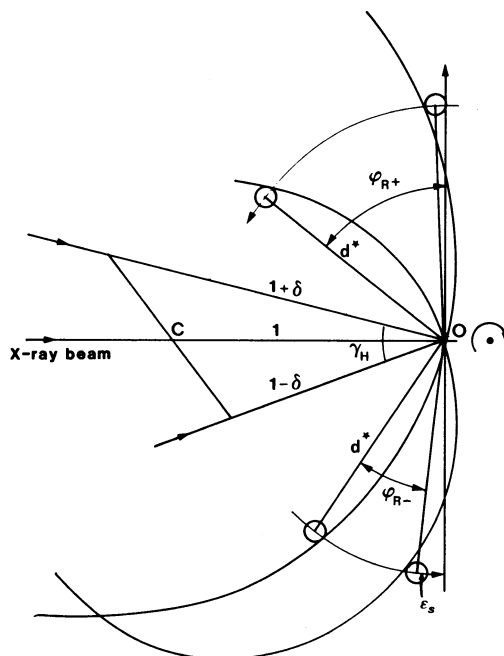
Fig. 2.2.7.4. The rocking width of an individual reflection for the case of Fig. 2.2.7.2(c) and a vertical rotation axis. φ_R is determined by the passage of a spherical volume of radius ε_s (determined by sample mosaicity and a conventional-source-type spectral spread) through a nest of Ewald spheres of radii set by $\delta = \frac{1}{2}[\delta\lambda/\lambda]_{corr}$ and the horizontal convergence angle γ_H. From Greenhough & Helliwell (1982).
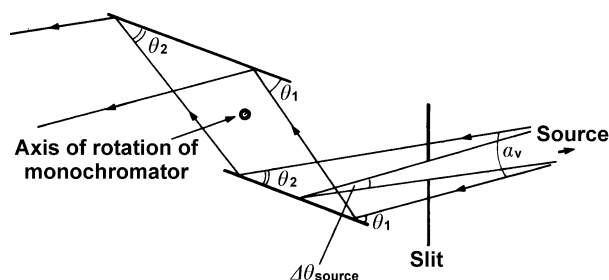

Fig. 2.2.7.3. Double-crystal monochromator illuminated by synchrotron radiation. The contributions of the source divergence α_V and angular source size $\Delta\theta_{source}$ to the range of energies reflected by the monochromator are shown.

(Subsection 2.2.3.4). For example, $\Delta\varphi_{max}$ may be 1.5° for a protein, and 0.4° or so for a virus. Many reflections will be only partially stimulated over the exposure. It is important, especially in the virus case, to predict the degree of penetration of the relp through the Ewald sphere. This is done by analysing the interaction of a spherical volume for a given relp with the Ewald sphere. The radius of this volume is given by

$$E \simeq \frac{\varphi_R}{2L} \qquad (2.2.7.14)$$

(Greenhough & Helliwell, 1982). For discussions, see Harrison, Winkler, Schutt & Durbin (1985) and Rossmann (1985).

In Fig. 2.2.7.4, the relevant parameters are shown. The diagram shows $(\delta\lambda/\lambda)_{corr} = 2\delta$ in a plane, usually horizontal, with a perpendicular (vertical) rotation axis, whereas the formula for φ_R above is for a horizontal axis. This is purely for didactic reasons since the interrelationship of the components is then much clearer. For full details, see Greenhough & Helliwell (1982).

2.2.7.4. *Geometric effects and distortions associated with area detectors*

Electronic area detectors are real-time image-digitizing devices under computer control. The mechanism by which an X-ray photon is captured is different in the various devices available (*i.e.* gas chambers, television detectors, charge-coupled devices) and is different specifically from film or image plates. Arndt (1986 and Section 7.1.6) has reviewed the various devices available, their properties and performances. Section 7.1.8 deals with storage phosphors/image plates.

(a) *Obliquity*

In terms of the geometric reproduction of a diffraction-spot position, size, and shape, photographic film gives a virtually true image of the actual diffraction spot. This is because the emulsion is very thin and, even in the case of double-emulsion film, the thickness, g, is only ~ 0.2 mm. Hence, even for a diffracted ray inclined at $2\theta = 45°$ to the normal to the film plane, the 'parallax effect', $g \tan 2\theta$, is very small (see below for details of when this is serious). With film, the spot size is increased owing to oblique or non-normal incidence. The obliquity effect causes a beam, of width w, to be recorded as a spot of width

$$w' = w \sec 2\theta. \qquad (2.2.7.15)$$

For example, if $w = 0.5$ mm and $2\theta = 45°$, then w' is 0.7 mm. With an electronic area detector, obliquity effects are also present. In addition, the effects of parallax, point-spread factor, and spatial distortions have to be considered.

(b) *Parallax*

In the case of a one-atmosphere xenon-gas chamber of thickness $g = 10$ mm, the $g \tan 2\theta$ parallax effect is dramatic [see Hamlin (1985, p. 435)]. The wavelength of the beam has to be considered. If a λ of ~ 1 Å is used with such a chamber, the photons have a significant probability of fully traversing such a gap and parallax will be at its worst; the spot is elongated and the spot centre will be different from that predicted from the geometric centre of the diffracted beam. If a λ of 1.54 Å is used then the penetration depth is reduced and an effective g, *i.e.* g_{eff}, of ~ 3 mm would be appropriate. The use of higher pressure in a chamber increases the photon-capture probability, thus reducing g_{eff} *pro rata*; at four atmospheres and $\lambda = 1.54$ Å, parallax is very small.

In general, we can take account of obliquity and parallax effects whereby the measured spot width, in the radial direction, is w'', where

$$w'' = w \sec 2\theta + g_{eff} \tan 2\theta. \qquad (2.2.7.16)$$

As well as changing the spot size, the spot position, *i.e.* its centre, is also changed by both obliquity and parallax effects by $\frac{1}{2}(w'' - w)$. The spherical drift-chamber design eliminated the effects of parallax (Charpak, Demierre, Kahn, Santiard & Sauli, 1977). In the case of a phosphor-based television system, the X-rays are converted into visible light in a thin phosphor layer so that parallax is negligible.

(c) *Point-spread factor*

Even at normal incidence, there will be some spreading of the beam size. This is referred to as the point-spread factor, *i.e.* a single pencil ray of light results in a finite-sized spot. In the TV-detector and image-plate cases, the graininess of the phosphor and the system imaging the visible light contribute to the point-spread factor. In the case of a charge-coupled device (CCD) used in direct-detection mode, *i.e.* X-rays impinging directly on the silicon chip, the point-spread factor is negligible for a spot of typical size. For example, in Laue mode with a CCD used in this way, a 200 μm diameter spot normally incident on the device is not measurably broadened. The pixel size is ~ 25 μm. The size of such a device is small and it is used in this mode for looking at portions of a pattern.

(d) *Spatial distortions*

The spot position is affected by spatial distortions. These non-linear distortions of the predicted diffraction spot positions have to be calibrated for independently; in the worst situations, misindexing would occur if no account were taken of these effects. Calibration involves placing a geometric plate, containing a perfect array of holes, over the detector. The plate is illuminated, for example, with radiation from a radioactive source or scattered from an amorphous material at the sample position. The measured positions of each of the resulting 'spots' in detector space (units of pixels) can be related directly to the expected position (in mm). A 2D, non-linear, pixel-to-mm and mm-to-pixel correction curve or look-up table is thus established.

These are the special *geometric* effects associated with the use of electronic area detectors compared with photographic film or the image plate. We have not discussed non-uniformity of response of detectors since this does not affect the geometry. Calibration for non-uniformity of response is discussed in Section 7.1.6.

references